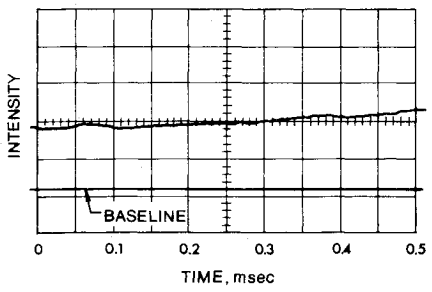

Fig. 3 Typical oscillogram, photomultiplier current vs time.

and the cathode was focussed on a photomultiplier. Periodic variation in the photomultiplier output signal would indicate the presence of a rotating spoke. Further discussion of the optical technique and equipment is given in Ref. 10.

This investigation was carried out for argon mass flow rates of 0.04-0.12 g/sec, exhaust tank pressures of 2.0×10^{-2}-7.5×10^{-2} torr, currents of 70-200 A, and magnetic field strengths of 0.0-0.24 tesla.

Results and Discussion

No periodic intensity oscillations, except those attributed to the 180 Hz power supply ripple, were observed for any combination of operating conditions. Specifically, no oscillations were present in the 25-300 kHz range expected for rotating spoke discharges. A copy of a typical oscillogram, showing luminous intensity as a function of time, is given in Fig. 3.

These results were somewhat surprising in light of the previous reports which predicted critical magnetic fields in the 0.1-0.2 tesla range, with spoke rotational frequencies on the order of 50 kHz for the reported operating conditions. The possibility of insufficient oscilloscope response was checked by replacing the initial 300 kHz bandwidth instrument with another oscilloscope having an upper frequency limit of 150 MHz. Possible inhibition of spoke operation by relatively large power supply ripple was also considered. A capacitive filter was inserted in the power supply output circuit to reduce the ripple by approximately one order of magnitude. The additional experiments confirmed the absence of periodic oscillations for the range of operating conditions considered.

The primary difference between the present experimental accelerator and those of the previously mentioned authors was in the cathode design. A consideration of the strong temperature dependence of electron emission and the thermal profile of the simple hollow cathode would suggest that this design would exhibit substantially more stable attachment than the more common conical design.

We suggest that the observed cathode spot stability may have had a direct effect on the discharge mode, maintaining a uniform discharge in an operating region where spoke mode operation has been observed by previous authors. This result merits further study since the discharge mode may have a direct effect on the electrode lifetime and the operating efficiency of a plasma accelerator.

References

[1] Connolly, D. J., Sovie, R. J., Michels, C. J., and Burkhart, J. A., "Low Environmental Pressure MPD Arc Tests," *AIAA Journal*, Vol. 6, July 1968, pp. 1271-1276.

[2] Malliaris, A. C., "Oscillations in an MPD Accelerator," *AIAA Journal*, Vol. 6, Aug. 1968, pp. 1575-1577.

[3] Larson, A. V., "Measurements of Plasma Flow in an MPD Engine," AIAA Paper 69-233, Williamsburg, Va., 1969.

[4] Allario, F., Jarrett, O., Jr., and Hess, R. V., "Onset of Rotating Disturbance in the Interelectrode Region and Exhaust Jet of an MPD Arc," *AIAA Journal*, Vol. 8, May 1970, pp. 902-907.

[5] Cochran, R. A. and Fay, J. A., "Occurence and Behavior of Current Spokes in MPD Arcs," *AIAA Journal*, Vol. 9, May 1971, pp. 886-893.

[6] Kribel, R., Eckdahl, C., and Lovberg, R., "Properties of the Rotating Spoke in an Unstable Pulsed MPD Arc," *AIAA Journal*, Vol. 9, May 1971, pp. 893-899.

[7] Fay, J. A. and Cochran, R. A., "An Actuator-Disk Model for Azimuthally Non-Uniform MPD Arcs," *AIAA Journal*, Vol. 7, Sept. 1969, pp. 1688-1692.

[8] Hassan, H. A. and Thompson, C. C., "Onset of Instabilities in Coaxial Hall Current Accelerators," AIAA Paper 69-230, Williamsburg, Va., 1969.

[9] Smith, J. M., "Electrothermal Instability—An Explanation of the MPD Arc Thruster Rotating Spoke Phenomenon," AIAA Paper 69-231, Williamsburg, Va., 1969.

[10] Collier, R. P. and Scott, D. S., "Simple Spectroscopic Technique for the Arc Region of Plasma Accelerators," *AIAA Journal*, Vol. 12, Jan. 1974, pp. 103-105.

Turbulence-Model Predictions for a Flat Plate Boundary Layer

Doyle Knight*

California Institute of Technology, Pasadena, Calif.

Introduction

RESEARCH with the turbulence model equations of Saffman on a variety of incompressible and compressible flows has met with considerable success.[2-6] In this instance, the model equations were employed in a calculation of the downstream development of mean flow quantities in a flat plate, zero-pressure-gradient, incompressible turbulent boundary layer—a problem not considered previously.

A. The Turbulence Model Equations for an Incompressible, Zero-Pressure Gradient Boundary Layer

Using the boundary-layer approximation, the Reynolds shear stress is postulated to satisfy the following constitutive relation[1]

$$-\overline{uv}=A(e/\omega)(\partial U/\partial y) \tag{1}$$

where e is the turbulence kinetic energy, and ω is a pseudo-vorticity. The transport equations for e and ω, employing the boundary-layer approximation, are the following:

$$U\frac{\partial e}{\partial x}+V\frac{\partial e}{\partial y}=\alpha''e\left|\frac{\partial U}{\partial y}\right|$$
$$-e\omega+\frac{\partial}{\partial y}\left[(A'\frac{e}{\omega}+\nu)\frac{\partial e}{\partial y}\right] \tag{2}$$
$$U\frac{\partial \omega^2}{\partial x}+V\frac{\partial \omega^2}{\partial y}=\alpha'\omega^2\left|\frac{\partial U}{\partial y}\right|$$
$$-\beta'\omega^3+\frac{\partial}{\partial y}\left[(A''\frac{e}{\omega}+\nu)\frac{\partial \omega^2}{\partial y}\right] \tag{3}$$

where ν is the kinematic viscosity. The constants appearing in the previous equations are given the following values:[1] $A=0.09$; $A'=A''=0.045$; $\beta'=5/3$; $\alpha''=0.3$; $\alpha'=0.163$. It

Received October 10, 1974; revision received February 6, 1975. I wish to express my appreciation to D. Brabston, H. B. Keller, P. G. Saffman, and H. Yuen for their assistance. This work was supported by the National Science Foundation and the Air Force Office of Scientific Research under Contract AFOSR 712092.

Index category: Boundary Layers and Convective Heat Transfer—Turbulent.

*Graduate Student; presently, Computational Aerodynamicist, Flight Dynamics Laborartory (FXM), Wright-Patterson Air Force Base, Ohio.

is important to note that these values were fixed by rather simple arguments,[1] and have *not* been optimized for any set of flows (the value of α' is chosen to make von Karman's constant $\kappa=0.41$). The additional equations are the conservation of mass and momentum

$$\frac{\partial U}{\partial x}+\frac{\partial V}{\partial y}=0 \tag{4}$$

$$U\frac{\partial U}{\partial x}+V\frac{\partial U}{\partial y}=\frac{\partial}{\partial y}\left(-\overline{uv}+\nu\frac{\partial U}{\partial y}\right) \tag{5}$$

The boundary conditions appropriate to this problem are the following.[1]:

1) At $y=y_m$, outside the viscous sublayer ($y_m u_*/\nu>50$):

$$U=(u_*/\kappa)\ell n(y_m u_*/\nu)+C$$

$$e=(\alpha''/A)u_*^2;\ \omega=\alpha'' u_*/\kappa y_m \tag{6}$$

where $u_*=(\tau_w(x)/\rho)^{1/2}$ is the local friction velocity and $C=5.0$.[7] The assumption of a similarity profile for the mean velocity in the sublayer, $U=u_*(x)f(yu_*(x)/\nu)$, yields, from the continuity equation

$$V+y_m(U/u_*(x))\ (du_*/dx)=0 \text{ at } y=y_m$$

2) As $y\to\infty$: $U\sim U_\infty$, $e\sim 0$, and $\omega\sim 0$.

B. Details of the Numerical Solution

The preceding set of parabolic differential equations were solved using the finite difference scheme of Keller.[8] The scheme has second-order accuracy with nonuniform mesh spacing; furthermore, Richardson extrapolation is valid and yields two orders of accuracy improvement per extrapolation (with nonuniform nets).

The data of Klebanoff[9] was used to provide an initial profile for the dependent variables. The Reynolds number based on the initial boundary-layer thickness was $6.59\ 10^{+4}$, and the initial skin friction coefficient was $2.73\ 10^{-3}$.

The initial profile was covered by 52 mesh points, of which 19 lay outside the boundary layer. The numerical scheme permitted the boundary layer to grow downstream, adding mesh points in the y-direction in order to maintain at least 6 points above the boundary layer at all downstream stations.

A value of $y_m=0.0375\ \delta_i$ (δ_i=initial boundary-layer thickness) was used, corresponding to $y_m u_*/\nu=91$. at $x=0$ (i.e., at the initial profile). A run with $y_m=0.0357\ \delta_i$ was made, with essentially the same results for downstream variables.

Because of the presence of ω in the denominator of the eddy viscosity, the boundary condition on ω at the top mesh point was taken as

$$\omega(x,\infty)=2\omega(0,\infty)/(2+\beta' x\omega(0,\infty)U_\infty^{-1}) \tag{7}$$

where $\omega(0,\infty)$ was taken to be $0.0374\ \omega(0,y_m)$. Equation (7) is a solution of the approximate form of Eq. (3) at $y\gg\delta$, namely

$$U_\infty d\omega^2/dx\doteq-\beta'\omega^3$$

To damp out small oscillations in the dependent variables outside the boundary layer, $e(x,\infty)$ was taken to be $4.0\ 10^{-6}\ U_\infty^2$ which corresponds to a turbulence intensity $T=(\frac{2}{3}e/U_\infty^2)^{1/2}=0.00164$. The shear stress was calculated on the assumption of a constant-stress sublayer. The formula is

$$c_f=\frac{\tau_w(x)}{\frac{1}{2}\rho U_\infty^2}=\frac{2A}{U_\infty^2}\frac{e}{\omega}\frac{\partial U}{\partial y}\Big|_{y=y_m} \tag{8}$$

which is consistent with the boundary conditions in Eq. (6).

For the first 40 downstream stations only, increments in x of $0.001\ \delta_i$ were taken and consecutive pairs of stations were averaged in x, the average values being placed at the midpoint of the two x-stations. The mesh size in x was gradually increased over the next 30 stations to $0.1\ \delta_i$, and the computation was ended at $x=91\ \delta_i$.

C. Results

Figure 1 indicates the downstream development of the shape factor (the ratio of displacement to momentum thickness). The contribution to these integrals from the region $0\leqslant y\leqslant y_m$ was obtained from the standard sublayer profiles of Coles[7] and the law of the wall, using the calculated value of the shear stress [i.e., Eq. (8)]. The shape factor decreases from an initial value of 1.393 to 1.328 at $x=30\ \delta_i$, and thereafter slowly declines to 1.287 at $x=91\ \delta_i$. Figure 1 also exhibits the calculated skin friction coefficient and the predicted values according to the skin friction law of Coles, which may be presented in the following form for an incompressible, fully developed flat-plate boundary layer with no pressure gradient:

$$c_f=2\left[\frac{\kappa}{\ln[\kappa(R_\delta^*-65)/(1+\Pi)]+C\kappa+2\Pi}\right]^2 \tag{9}$$

where $R_\delta^*=U_\infty\delta^*/\nu$, $\kappa=0.41$, $C=5.0$, and $\Pi=0.62$.[7]

The calculated skin friction rises by 1.43% from $x=0$ to $x=21\ \delta_i$, indicating a relaxation from the initial profiles. Various techniques were attempted to decrease or eliminate this relaxation, which is due to an incompatibility of the initial data and the model equations, but none were successful. From $x=21\ \delta_i$ onwards, the calculated skin friction is steadily decreasing, and at $x=91\ \delta_i$, $c_f=2.577\ 10^{-3}$. The value predicted by Coles' skin friction law [Eq. (9)] is $2.397\ 10^{-3}$ at $x=91\ \delta_i$, and the calculated data are within 7.6% of the predicted values at all x. The skin friction calculations were also compared with the skin friction law of Karman and Schoenherr[10]

$$c_f=\{17.08(\log_{10}R_\Theta)^2+25.11\log_{10}R_\Theta+6.012\}^{-1}$$

where Θ is the displacement thickness, $R_\Theta=U_\infty\Theta/\nu$. The calculated values of c_f agreed to within 6.4% for all x. The initial profiles of turbulence energy and shear stress, and the calculated profiles at $x=90\ \delta_i$ are shown in Fig. 2. Note that

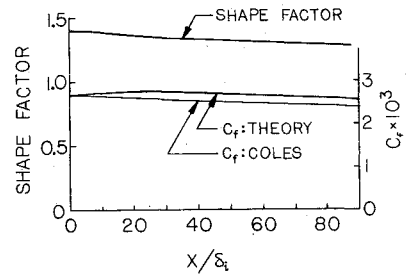

Fig. 1 Downstream variation of shape factor and skin friction.

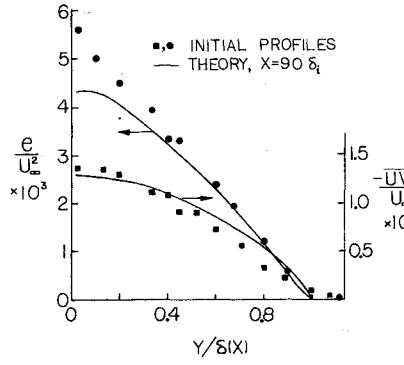

Fig. 2 Initial and final turbulence energy and Reynolds stress profiles.

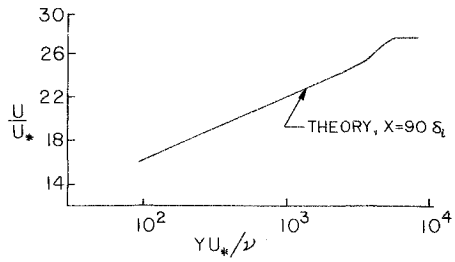

Fig. 3 Mean velocity profile in wall variables.

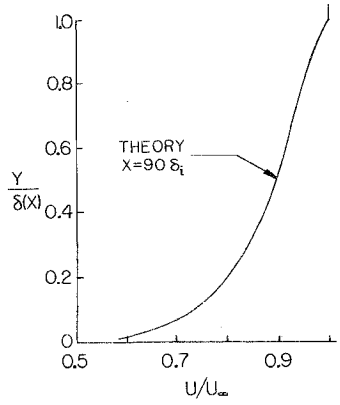

Fig. 4 Mean velocity profile in outer variables.

both variables exhibit a sharp interface or superlayer at $y=\delta(x)$.[3] In Fig. 3, the mean velocity at $x=90\,\delta_i$ is plotted in wall variables. Within the region of validity of the law of the wall, the calculated profile is within 1% of the log profile

$$U/u_* = (1/\kappa)\,\ell n\,(yu_*/\nu) + C$$

where $\kappa=0.41$, $C=5.0$, and u_* is calculated from Eq. (8). The combined law of the wall and wake

$$U/u_* = (1/\kappa)\,\ell n\,(yu_*/\nu) + C + (2\Pi/\kappa)\sin^2(\pi y/2\delta)$$

(where $\Pi=0.62$ for a flat-plate zero pressure gradient turbulent boundary layer[8]) implies a relation between the skin friction and boundary-layer thickness, and therefore the small error in calculating c_f (Fig. 1) precludes comparison with the velocity profile in the wake region. Furthermore, the combined law of the wall and wake, being an unconditional average taken at a fixed distance from the wall, embodies the intermittent structure of the outer region of the boundary layer. The model equations, however, assume no intermittency, and it would therefore be more appropriate to compare the calculated mean velocity as well as the calculated mean turbulence quantities in the outer region with conditional turbulent averages taken at fixed distances from the instantaneous edge of the boundary layer. Such measurements have apparently not been published to date. The mean velocity at $x=90\,\delta_\theta$ is replotted in Fig. 4 in outer variables to display its sharp superlayer at $y=\delta$.

References

[1]Saffman, P. G., "Model Equations for Turbulent Shear Flow," *Studies in Applied Mathematics*, Vol. 53, March 1974, pp. 17-34.

[2]Saffman, P. G. and Wilcox, D. C. "Turbulence-Model Predictions for Turbulent Boundary Layers," *AIAA Journal*, Vol. 12, April 1974, pp. 541-546.

[3]Saffman, P. G., "A Model for Inhomogeneous Turbulent Flow," *Proceedings of the Royal Society (London)*, Vol. A317, 1970, pp. 417-433.

[4]Knight, D. D., "An Analytical Investigation of Turbulent Flow Over a Wavy Boundary," Ph.D. thesis, 1974, Department of Aeronautics, California Institute of Technology, Pasadena, Calif.

[5]Wilcox, D. C. and Alber, I. E., "A Turbulence Model for High Speed Flows," *Proceedings of the 1972 Heat Transfer and Fluid Mechanics Institute*, Stanford Univ. Press, Stanford, Calif. 1972.

[6]Wilcox, D. C., "Calculation of Turbulent Boundary Layer Shock Interaction," *AIAA Journal*, Vol. 11, Nov. 1973, pp. 1592-1594.

[7]Coles, D., "The Young Person's Guide to the Data," *AFOSR-IFP-Stanford Conference on Computation of Turbulent Boundary Layers*, Vol. II,Stanford University Press, Stanford, Calif. 1968.

[8]Keller, H., "A New Difference Scheme for Parabolic Problems," *Numerical Solution of Partial Differential Equations—II*, edited by B. Hubbard, Academic Press, New York, 1970, pp. 327-350.

[9]Klebanoff, P. S., "Characteristics of Turbulence in a Boundary Layer with Zero Pressure Gradient," Rept. 1247, May 1953, NACA.

[10]Hopkins, E. J. and Inouye, M., "An Evaluation of Theories for Predicting Turbulent Skin Friction and Heat Transfer on Flat Plates at Supersonic and Hypersonic Mach Numbers," *AIAA Journal*, Vol. 9, June 1971, pp. 993-1003.

Holographic Analysis of Particle-Induced Hypersonic Bow-Shock Distortions

D.T. Hove* and A.A. Smith†

Science Applications, Inc., El Segundo, Calif.

Introduction

BACKFACE temperature measurements made on thin skin blunt models subjected to dust-laden, hypersonic flows have indicated significantly enhanced stagnation region heating rates over clear air values.[1-3] High-speed shadowgraph movies taken in hypersonic wind tunnels and laser photographs taken in ballistic ranges revealed that the model bow shocks were severely distorted by the particulate in the flow. The bow shock distortions generally had the appearance of large-angle conical shocks which traveled upstream from the bow shock and then collapsed or were swept around the model. Previous investigators[2,3] postulated that the shock distortions were initiated by rebounding dust particles or model ejecta and that the large cone angles were due to communication with the high pressure bow-shock region through the particle wakes.

Tests were performed in the Boeing Hypersonic Wind Tunnel in a Mach 5 combined dust particle/aerodynamic flow environment to investigate the particle-induced bow-shock distortions and their connection with enhanced stagnation region heating rates. As part of the test program, three-dimensional laser holograms were obtained to examine the structure of the bow-shock distortions.

Experiment Description

An in-line laser holocamera mounted perpendicular to the wind tunnel centerline viewed the models through 15-cm optical windows. Coherent light from a 30-millijoule Q-switched ruby laser was used to illuminate the particle field and test model. Duration of the laser pulse was about 15 nsec which effectively froze the particle and shock distortion motion.

The laser power source was charged when the tunnel conditions were being established, and the laser was fired manually about a second after the model reached the tunnel centerline. Holograms were taken of 12 dust tests including two model sizes and materials (2.5 and 6.0 cm titanium and graphite disks), two flow unit Reynolds number (2.8 and

Received October 23, 1974; revision received December 23, 1974. This work was sponsored by the Air Force Space and Missile Systems Organization (SAMSO) under Contract FO4701-73-C-0095.

Index categories: Boundary Layers and Convective Heat Transfer—Turbulent; Shock Waves and Detonations; Supersonic and Hypersonic Flow.

*Staff Scientist. Member AIAA.

†Optical Technician, Tullahoma, Tenn.